[Article] DOI: 10.13208/j.electrochem.2213008 Http://electrochem.xmu.edu.cn

Mechanism and Application of Nickel Nano-Cone by Electrodeposition on a Flexible Substrate

Xiu-Ren Ni[1], Ya-Ting Zhang[1], Chong Wang[1], Yan Hong[1*], Yuan-Ming Chen[1], Yuan-Zhang Su[1], Wei He[1], Xian-Ming Chen[2], Ben-Xia Huang[2], Zhen-Lin Xu[3], Yi-Feng Li[3], Neng-Bin Li[3], Yong-Jie Du[4]

(*1. School of Materials and Energy, University of Electronic Science and Technology of China, Chengdu 610054, Sichuan, China; 2. Zhuhai ACCESS Semiconductor Co., Ltd, Zhuhai 519175, Guangdong, China; 3. Xiamen Institute of Flexible Electronics Co., Ltd & Xiamen Hongxin Electron-Tech Co., Ltd, Xiamen 361101, Fujian, China; 4. Zhuhai Dynamic Technology Optical Industry Co., Ltd,Zhuhai 519175, Guangdong, China*)

Abstract: Nano-array structure possesses promising prospect in power supply, optical device and electronic manufacturing. In this paper, a black nickel nano-cone array was prepared on a flexible substrate by galvanostatic deposition and the corresponding factors involved in the fabrication of nickel nano-cone array was explored. Experimental results showed that a large current density and low main salt concentration were not favored to the formation of cone nickel structure. It was also found that ammonium chloride, as the crystal modifier, was crucial to deposit the uniform nano-cone array. In addition, the growth mechanism of nickel nano-cone was further studied by molecular dynamics simulation. The excellent wettability and light absorption of nickel nano-cone array were investigated, which demonstrates potential applications of the nickel nano-cone array.

Key words: nickel nano-cone array; electrodeposition; molecular dynamics simulation; flexible

1 Introduction

Nano-array materials have drawn widespread attention due to the unique mechanical, optical and electrical properties[1-3]. The structure of nano-array has displayed promising prospects in electronic manufacturing, catalytic application and interfacial interaction[4-7]. Various techniques to prepare nano-array materials have been proposed. The fabrication of nano-array is mainly conducted by photolithography, template method and chemical vapor deposition (CVD)[8-10]. However, these methods can hardly fulfill the needs of manufacturing application due to the high cost, stringent device-dependence and low efficiency.

Electrodeposition, as a low cost and convenient method, has been widely used in the preparations of metal coatings and interconnection[11-17]. Specific morphology and crystal surface in nanoscale can be established by controlling electroplating parameters and additives without the existence of templates[18-20]. Template-free one-step electroplating to build the aligned single-crystal copper nano-cones on the copper surfaces has been reported[21]. The copper nano-cones provide high-efficiency boiling heat transfer interfaces and display an excellent heat transfer per-

Cite as: Ni X R, Zhang Y T, Wang C, Hong Y, Chen Y M, Su Y Z, He W, Chen X M, Huang B X, Xu Z L, Li Y F, Li N B, Du Y J. Mechanism and application of the nickel nano-cone by electrodeposition on flexible substrate. *J. Electrochem.*, 2022, 28(7): 2213008.

Received: 2022-05-06, Revised: 2022-06-06. *Corresponding author, Tel: (86-28)61830951, E-mail: hongyan@uestc.edu.cn

formance. Compared with copper, nickel is widely applied in anti-corrosion, decoration and superalloy materials because of the outstanding heat-resistance, mechanical stability and corrosion resistance[4, 22]. Nickel foil in nanoscale was prepared in the sulfamate-based electrolyte and the mechanical properties of nickel nanocrystal were discussed[23]. Yin et al. obtained the highly ordered parallel hexagonal Ni and Bi nanowires by electrodeposition in an organic bath of dimethyl sulfoxide with metal chloride as the electrolyte[19]. Elsherik et al. successfully developed nickel nanocrystal with a size of 10 nm ~ 40 nm by pulse electroplating in saccharin-containing electroplating solution. Uniformly distributed nickel nanocrystal was obtained by controlling the electroplating conditions including the pulse switching time, peak current density, pH and temperature of the plating solution[24, 25]. However, the growth mechanism and theoretical calculation of nano-arrays are still inadequate, and researches on the specific application of nano-arrays are insufficient.

In this paper, a uniform nickel nano-cone array layer was prepared by one-step electrodeposition method, and the influences of current density and salt concentration, especially for the crystal modifier, on the morphology of electrodeposited nickel nano-cone array were studied. Notably, the growth mechanism of nickel nano-cone array was studied by multiple characterization and molecular dynamics simulation. The unique optical and interfacial properties were investigated by ultraviolet-visible diffuse reflectance spectroscopy and the contact angle tests. The nickel nano-cone array was prepared on the flexible substrates, which exhibited excellent wettability and more than 95% near ultraviolet adsorption.

2 Experimental

2.1 Electrodeposition

The nickel nano-cone array was prepared by electrodeposition in a 500 mL bath containing main salt $NiCl_2 \cdot 6H_2O$, and crystal modifier NH_4Cl and H_3BO_3. The nickel plate wrapped with filter paper and flexible copper-clad laminate (CCL) were used as the anode and cathode, respectively. The electroplating experiment was carried out with a constant current of 0.5 ~ 4.0 A·dm^{-2} and the temperature of solution was 50 ℃. The electrodeposited solution was agitated by magnetic stirring. The flexible CCL was cleaned by the pretreatment process including alkaline washing (OP-200), etching and 5% sulfuric acid washing to remove the oil stain and attachments on the CCL surface. The etching solution was obtained by adding 5% volume fraction sulfuric acid and 5 % ammonium persulfate. The temperatures of alkaline washing, etching and acid washing were 50 ℃, 25 ℃ and 25 ℃, respectively.

2.2 Molecular Dynamics Simulation

The adsorption behavior of crystal modifier on different nickel crystal surfaces is calculated by molecular dynamic (MD) simulation. A simulation box containing 100 water molecules, six ammonium ion and six layers of nickel ions is established. The results is obtained by BIOVIA Materials studio and the geometry optimization is conducted by COMPASS force field in Forcite tools, which is suitable for simulate the interaction between metal crystal and additives[26-31]. The B3LYP correlation energy gradient correction functional method of density functional theory (DFT) is used to study the adsorption behavior and the base group is set as 6-311G (d, p). The summing method is set as Ewald electrostatic and Atom based van der Waals parameters, and monte Carlo method of the canonical ensemble (NTV) is used in the simulation. The temperature is 25 ℃, and the molecule number and volume of the system are constant. The adsorption energy and binding energy are calculated by following the formulas (2-3). Ecomplex, E_{Ni} and E_{ad} ditives represent the energy values of complex box including nickel layer and additives, only nickel layer box and only additives box, respectively.

$$E_{ack} = E_{complex} - (E_{Ni} + E_{additives}) \quad (1)$$

$$E_{binding} = - E_{ack} \quad (2)$$

2.3 Characterization

The morphology of electrodeposited nickel was observed by scanning electron microscope (SEM, HITACHI S3400) and the crystal orientation of the metal

surface was tested using X-ray diffractometer (XRD, Rigaku MINIFLEX 600). The JY-PHa contact angle tester was used to measure the contact angle and the contact angle was obtained by height measurement method[19]. The light absorption performance was investigated by solid ultraviolet-visible diffuse reflectance spectrometer (Shimadzu UV3600 plus). The light absorption results were obtained by Kubelka-Munk (KM), which describes the optical relationship of a beam of monochromatic light incident on an object that can both absorb and reflect light[32]. The K-M equations are displayed as the following equations (3-5), where R_∞ (the absolute reflectivity) represents the limit value of the reflection coefficient of the infinite thick sample. K and S represent the absorption coefficient and semi-scattering coefficient, respectively. $F(R_\infty)$ is called K-M coefficient. The ordinate of the absorbance test in this paper is the reflectivity ratio, which means that the intensity of the reflected light of the sample is relative to the reflection intensity of the reference sample ($BaSO_4$).

$$F(R_\infty) = \frac{K}{S} = \frac{(1-R_\infty)^2}{2R_\infty} \tag{3}$$

$$\log F(R_\infty) = \log K - \log S = \frac{(1-R_\infty)^2}{2R_\infty} \tag{4}$$

$$R_\infty = 1+\frac{K}{S} - \left[\frac{K^2}{S^2}+\frac{2K}{S}\right]^{\frac{1}{2}} \tag{5}$$

3 Results and Discussion

The nickel nano-cone array with width of 200 nm was electrodeposited on the flexible copper substrate. The electrodeposition parameter was optimized by orthogonal experiment and the uniform nickel nano-cone array was obtained in the solution with 1.68 mol·L^{-1} $NiCl_2$·$6H_2O$ and 4.0 mol·L^{-1} NH_4Cl. As shown in Figure 1a and 1b, the electrodeposited nickel nano-cone array distributed uniformly and the black nickel nano-cone layer with 1 μm height was developed. The nickel nano-cone was further characterized by TEM and XRD, and the center of the nickel nano-cone was investigated by high resolution transmission electron microscope, as displayed in Figure 1c and 1d. The center of nickel nano-cone in Figure 1c was deeper than the other areas due to the overlap of the edges of the nickel nano-cone structure. The crystal plane spacing of 0.205 nm was observed,

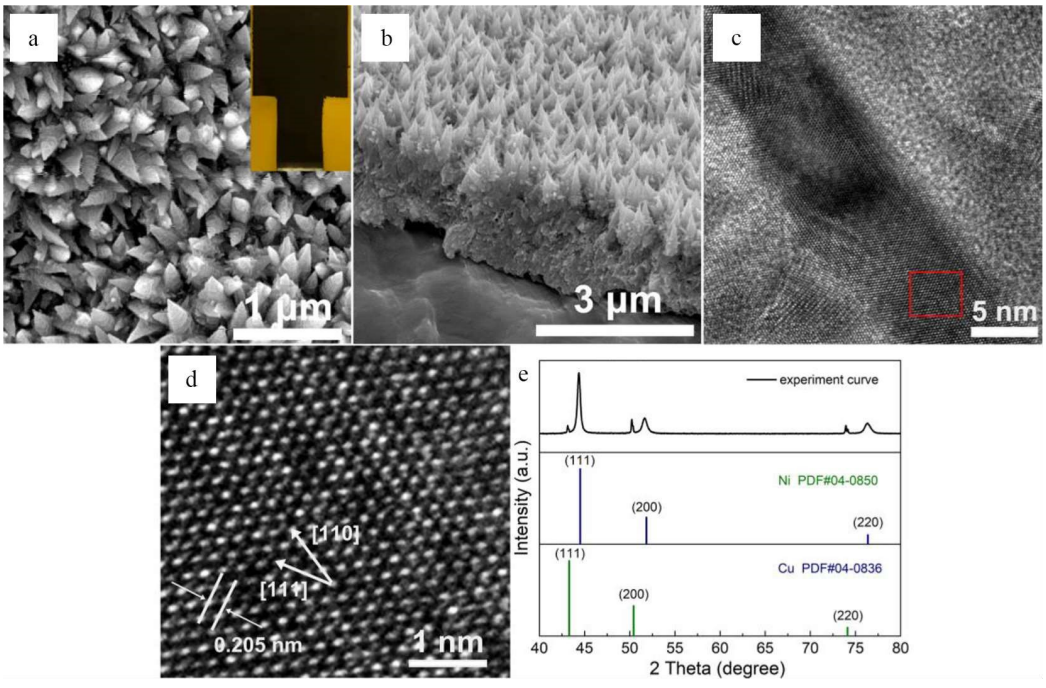

Figure 1 Characterization of the electrodeposited nickel nano-cone array. (a, b) SEM, (c) TEM, (d) HRTEM images, and (e) XRD patterns. (color on line)

which corresponds to the (111) plane of nickel and the growth direction of [110] (Figure 1d). The XRD patterns of the nickel nano-cone is also included in Figure 1e, displaying obvious diffraction peaks of the nickel nano-cone at 44.5°, 51.8° and 76.4°, corresponding to the (111), (200) and (220) planes of nickel with a face-centered cubic structure (PDF 04-0850), respectively.

Effect of main salt concentration on the morphology of electrodeposited nickel nano-cone was investigated. As shown in Figure 2a-2c, in the solution with 1.0 mol·L^{-1} NH_4Cl, the morphology of electrodeposited nickel changed from spindle to nano-cone. When the concentration of $NiCl_2·6H_2O$ reached to 1.68 mol·L^{-1} (Figure 2c), the nickel cone appeared uneven distribution. Notably, the nickel nano-cone was not obtained in the absence of NH_4Cl (Figure S1). As the nickel crystal modifier, ammonium ion provided by NH_4Cl is crucial for fabricating the nano-cone array. In addition, with the increase in the concentration of NH_4Cl, the particles of electrodeposited nickel became finer, leading to the formation of uniform nickel nano-cone array. When the concentration of NH_4Cl reached to 4 mol·L^{-1}, the nickel nano-cone array with the width of 200 nm and height of 1 μm was distributed uniformly and compactly on the flexible CCL. The results indicated that the morphology of electrodeposited nickel was refined by

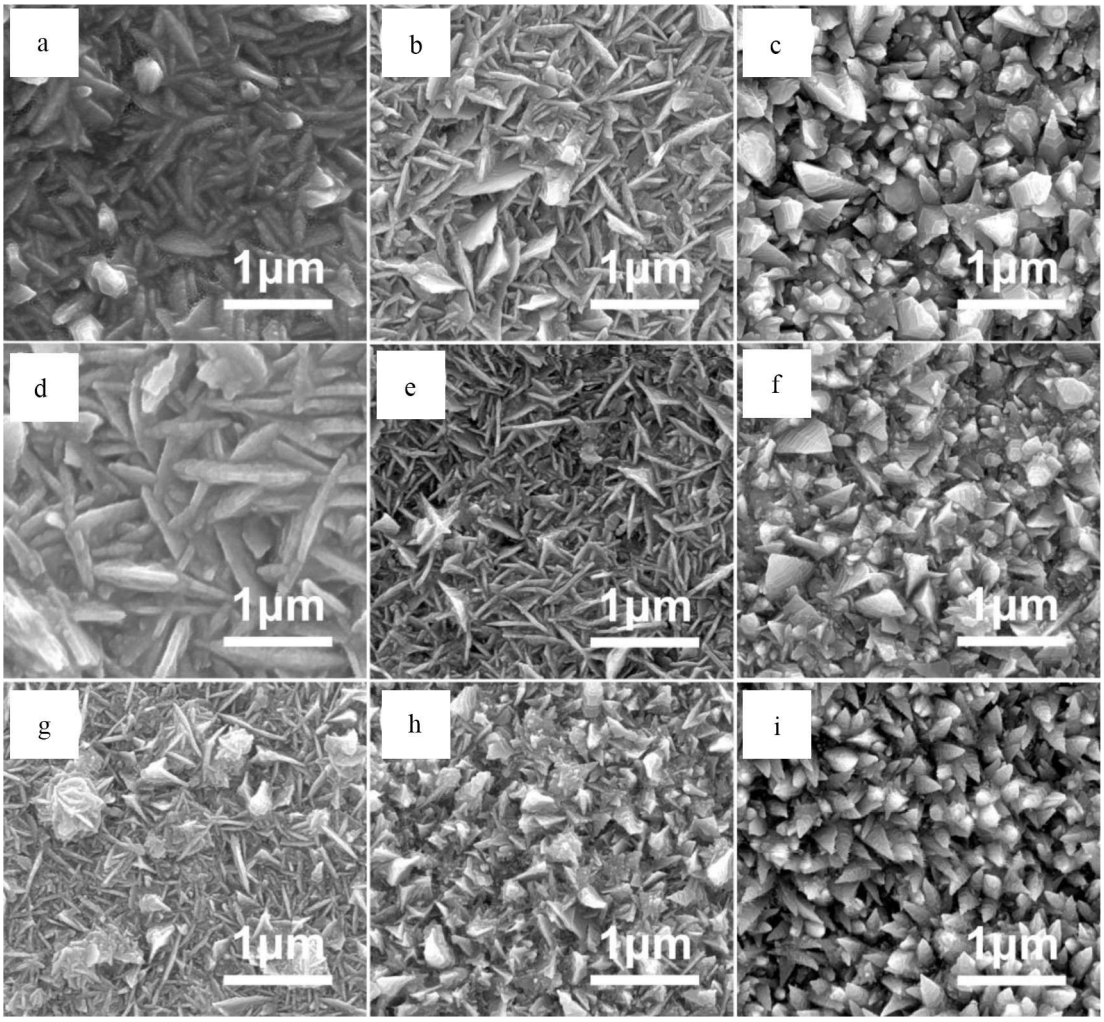

Figure 2 SEM images of the electroplated nickel nano-cone with different main salt concentrations (a, d, g) 0.42 mol·L^{-1}, (b, e, h) 0.84 mol·L^{-1}, (c, f, i) 1.68 mol·L^{-1} $NiCl_2·6H_2O$, and various crystal modifier concentrations (a, b, c) 1.0 mol·L^{-1}, (d, e, f) 2.0 mol·L^{-1}, (g, h, i) 4.0 mol·L^{-1} NH_4Cl.

adding $NiCl_2 \cdot 6H_2O$ and the nickel ions could be supplied immediately in the high concentration of $NiCl_2 \cdot 6H_2O$, which is conductive to the growth of nickel nano-cone nuclei. The nickel nuclei formed in the high concentration of $NiCl_2 \cdot 6H_2O$ provide sufficient active sites to form the nano-cone array. The uniform nickel nano-cone array was built in the solution with the addition of ammonium ion provided by NH_4Cl, which leads to a difference in the direction of crystal growth.

The effect of current density on the nickel nano-cone electrodeposition was also investigated, and the current density was chosen in the range of 1 $A \cdot dm^{-2}$ ~ 4 $A \cdot dm^{-2}$. The electrodeposited nickel nano-cone array was conducted in the solution containing 1.68 $mol \cdot L^{-1}$ $NiCl_2 \cdot 6H_2O$, 4 $mol \cdot L^{-1}$ NH_4Cl and 0.5 $mol \cdot L^{-1}$ H_3BO_3. The temperature of electrodeposition bath was 55 ℃. As shown in Figure 3a-3c, the nickel nano-cone was obtained when the current density was lower than 2 $A \cdot dm^{-2}$. However, the nano-cone disappeared and the rod-like structures in the agglomerated particles appeared when the current density continued to increase to 4 $A \cdot dm^{-2}$. Meantime, the color of the nickel coating changed into grey white from black. The nickel electrodeposition was accelerated at high current density, which results in the difference of nickel ion concentration on the electrode surface and far away from the electrode, leading to the increasing polarization. Besides, the adsorption behavior of crystal modifier was unstable. The nucleation and growth of nickel nano-cone was affected. Particularly, the current density needs to exceed the value of 1 $A \cdot dm^{-2}$ in nickel electrodeposition because of the nickel deposition potential and low growth rate at the current density below 1 $A \cdot dm^{-2}$.

The growth mechanism was explored by morphology characterization and molecule dynamic simulation. As shown in Figure 4, the morphology of the electrodeposited nickel nano-cone at different electrodeposition time is displayed, and the uniform nickel nano-cone was electrodeposited on the copper substrate. Figure 4a shows the SEM image of copper

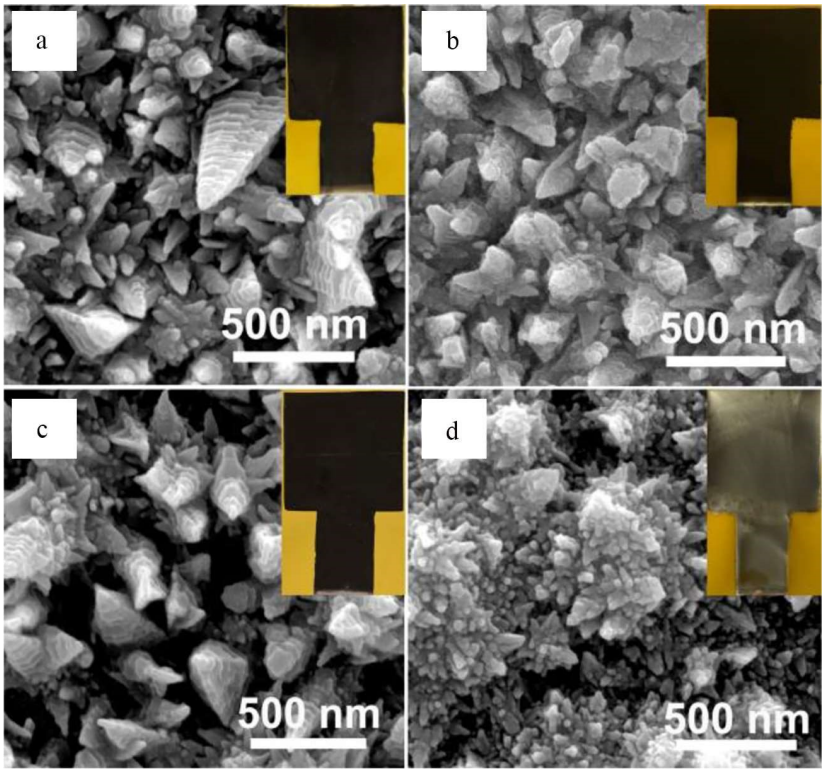

Figure 3 SEM images of the electroplated nickel nano-cone with different current densities. (a) 1 $A \cdot dm^{-2}$, (b) 1.5 $A \cdot dm^{-2}$, (c) 2 $A \cdot dm^{-2}$, (d) 4 $A \cdot dm^{-2}$. (color on line)

substrate and the copper particles were observed on the flat surface. After 10 s of nickel electrodeposition (Figure 4b), a large number of nickel nuclei were generated on the surface of copper and the nucleation process became faster than the nuclear growth process in this stage. With the increase of nickel electrodeposited time, the nickel nano-cone nucleus grew up and the nano-cone was more distinguishable. When the time of electrodeposited nickel continued to be increased, the nano-cone kept increasing and the complete nickel nano-cone array was obtained finally. In this stage, the nano-cone growth rate is greater than the nucleation rate, and the nickel nano-cone grows up gradually (Figure 4c-4e). Therefore, the two-stage-formation of nickel nano-cone array on a flexible copper substrate is proposed, including the nucleation and nuclei growth. In the nucleation stage, the rate of nucleation is faster than the nuclei growth, resulting in a large number of nickel nuclei occupied on copper surface which provides sufficient sites to form nickel nano-cone. Subsequently, the nickel nuclei continue to grow and the uniform nickel nano-cone array can be obtained.

The molecule dynamic simulation is performed to investigate the growth mechanism of nickel nano-cone array by calculating the adsorption energy of NH_4^+ on different crystal surfaces of nickel. As shown in Figure 5, NH_4^+ can be adsorbed on the surface of all the three crystal planes including the (111), (200) and (220) surfaces. The total energy, bond energy and non-bond energy of NH_4^+ on nickel (111), (200) and (220) crystal planes in the simulation box reach stable state after 50 ps of simulation, indicating that the adsorption state balances within 50 ps (Figure 5c, 5f, 5i). The values of adsorption energies and binding energies of NH_4^+ on nickel (111), (200) and (220) crystal planes are displayed in Table 1. The results indicate that the NH_4^+ has the lowest value of binding energy on the (220) crystal plane (14.14 kcal·mol^{-1}), and the binding energies of NH_4^+ on the nickel (111) and (200) planes are 19.10 kcal·mol^{-1} and 18.83 kcal·mol^{-1}, respectively. The smaller the value of binding energy, the weaker is the adsorption of additive[33-36]. The stronger adsorption behavior indicates that more NH_4^+ tends to be adsorbed on the surface

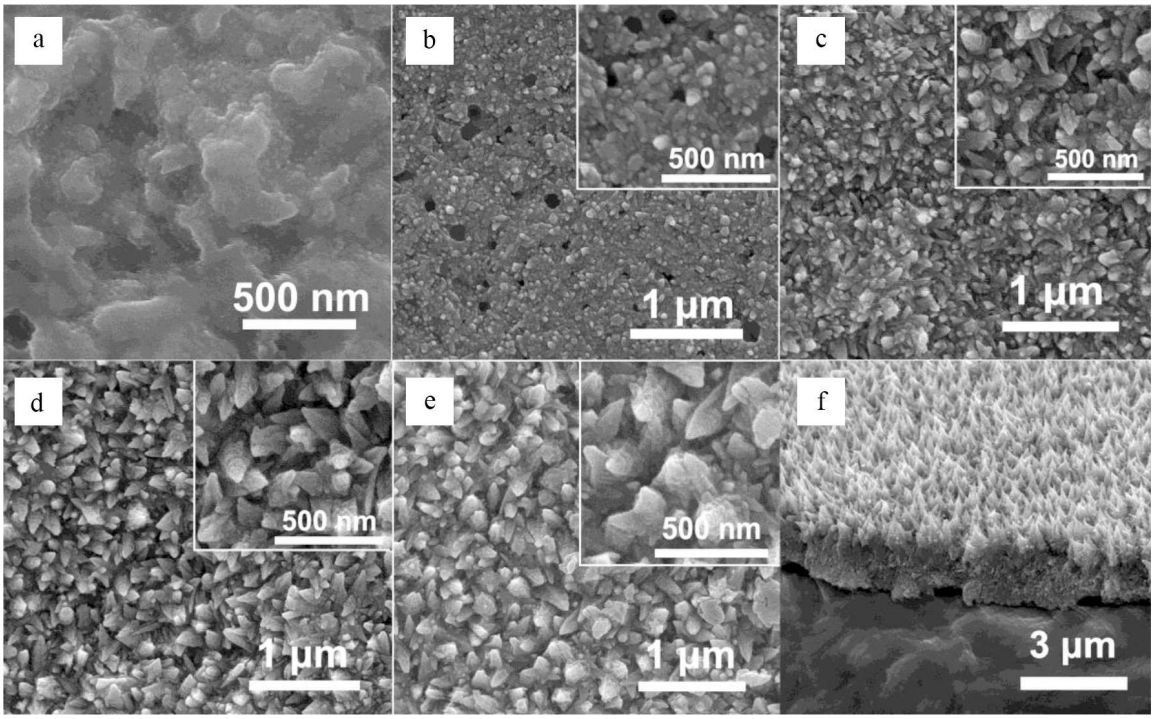

Figure 4 SEM images of the nickel nano-cone array at different electrodeposition time. (a) 0 s, (b) 10 s, (c) 20 s, (d) 100 s, (e, f) 300 s.

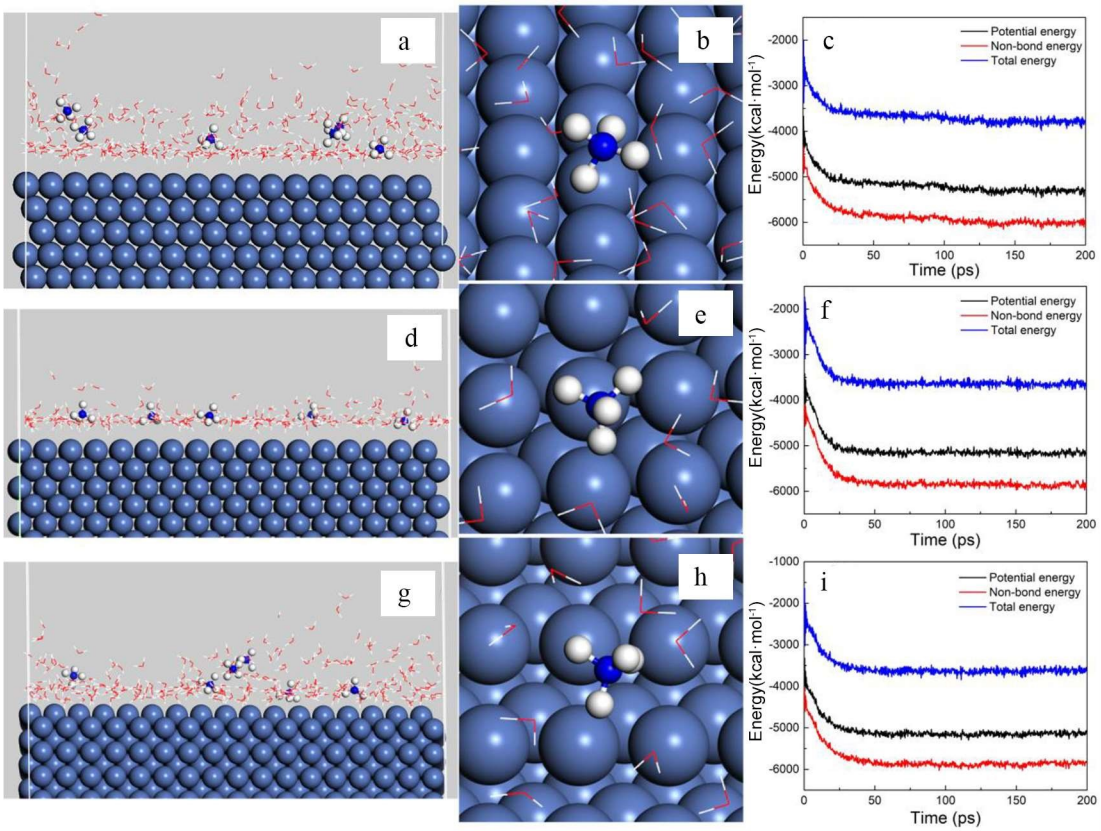

Figure 5 Molecule dynamic simulation of NH_4^+ on nickel (a-c) (111), (d-f) (200) and (g-i) (220) planes. (color on line)

Table 1 The adsorption energies of the NH_4^+ on different nickel crystal surfaces

	$E_{binding}$ (kcal·mol^{-1})	E_{ads} (kcal·mol^{-1})
NH_4^+ on Ni (111)	19.10	-19.10
NH_4^+ on Ni (200)	18.83	-18.83
NH_4^+ on Ni (220)	14.14	-14.14

and the growth of nickel on the surface is suppressed. Therefore, NH_4^+ has the weakest adsorption behavior on the surface of (220) compared with (111) and (200), leading to the growth along nickel [220] direction. Besides, the values of binding energy on the nickel (111) and (200) plane are near, which indicates the intensity of NH_4^+ adsorption is similar. Finally, the growth of nickel (111) and (200) is suppressed obviously and nickel nano-cone grows along [220] direction, which is consistent with the TEM results in Figure 1.

The properties of nickel nano-cone array were further explored. The nickel nano-cone array exhibits unique optical and interfacial properties. As shown in Figure 6, the water contact angles on polyimide (PI), Cu, Watt nickel and nickel nano-cone array were tested. The water contact angles of the PI, Cu and Watt nickel were 76.6°, 68° and 48.8°, respectively. However, the water contact angle of the nickel nano-cone array was only 5.4°, which indicates the excellent hydrophilicity of nano-cone array. The excellent wettability is conductive to the solid-liquid interface reaction[37]. The surface tension is reduced due to the widespread nano-grooves formed by the nano-cone array, leading to capillary action on the surface of the nickel.

The light adsorption performance of nickel nano-cone array was investigated by ultraviolet-visible diffuse reflectance spectrometer. The results confirmed that the light absorption efficiency in the near ultraviolet and visible light range was more than 95% (Figure 7). The nickel nano-cone at different current densi-

ties of electr odeposition was tested, and the nickel nano-cone array electrodeposited at 1.5 A·dm^{-2} had the best performance of light adsorption which adsorbed 95% near ultraviolet and visible light. It is reported that the light adsorption performance could be improved by adjusting the refractive index of the material[38-40]. The uniform nickel nano-cone array with the width of 300 nm at the bottom forms the equivalent refractive index transition layer. The equivalent refractive index gradient structure of nickel nano-cone array reduces the light reflection. The conductive nickel nano-cone array with distinctive light adsorption performance may has potential in photovoltaic and solar applications.

4 Conclusions

In this paper, the nickel nano-cone array layer was succ essfully prepared by electrodeposition and the factors that influenced the nickel nano-cone array electrodeposition were studied. It was found that high main salt concentration and low current density were beneficial to the formation of nickel nuclei, which provides sufficient sites to fabricate the nano-cone array. Ammonium chloride, as the crystal modifier, had the weakest adsorption behavior on the surface of nickel (220) compared with (111) and (200), leading to the predominant growth along nickel [220] direction. Besides, the nickel nano-cone array exhibited more than 95% light adsorption performance and ex-

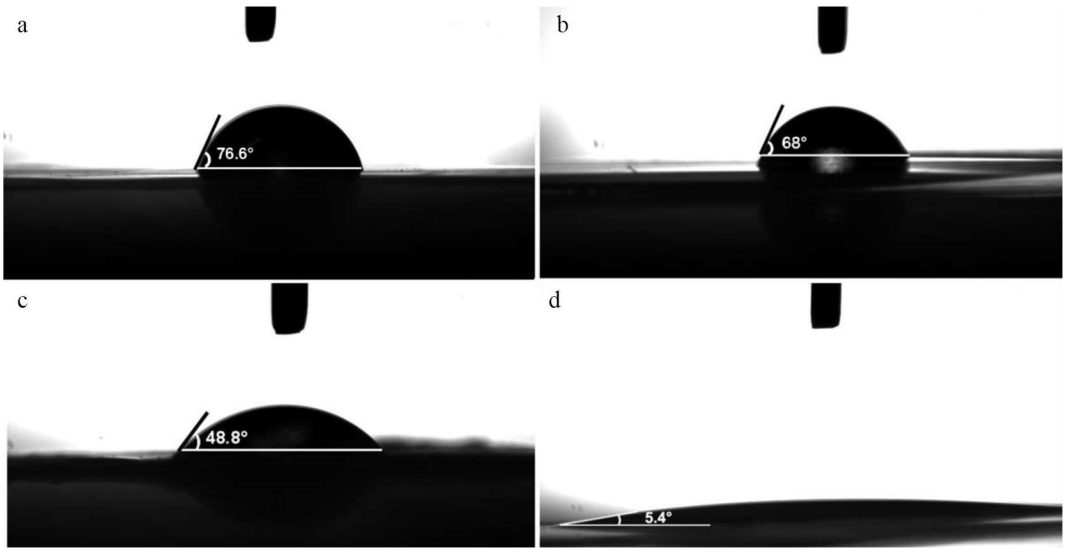

Figure 6 Water contact angles on different surfaces. (a) PI, (b) Cu, (c) Watt nickel, (d) nickel nano-cone substrate.

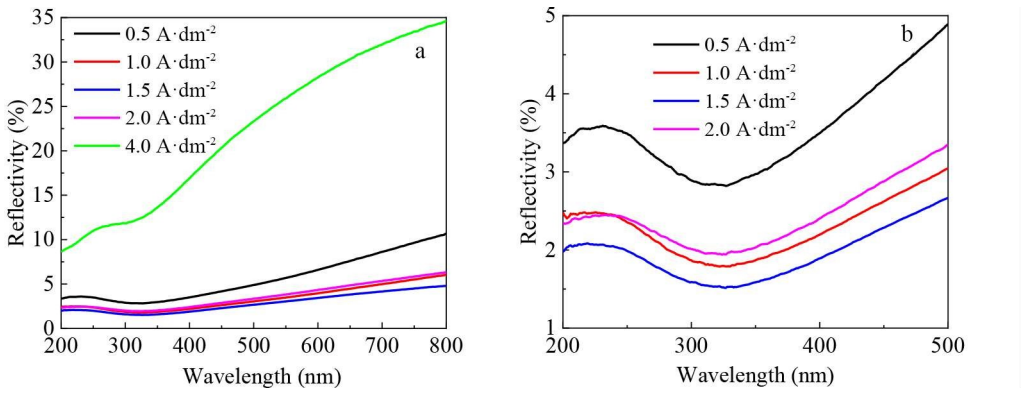

Figure 7 UV visible reflectance spectra of nickel nano-cone obtained at different current densities in the wavelength range of (a) 200 ~ 800 nm and (b) 200 ~ 500 nm. (color on line)

cellent hydrophily.

Acknowledgments:

The authors gratefully acknowledge the support of National Natural Science Foundation of China (Nos. 22172020 and 61974020). The work is also supported by the projects of Sci & Tech planning of Zhuhai City (No. $ZH_2$2017001200032PWC) and Sichuan Science and Technology Program (No. 2022YFS0527).

References:

[1] Wang F, Zuo Z C, Li L, He F, Li Y L. Graphdiyne nanostructure for high-performance lithium-sulfur batteries[J]. Nano Energy, 2020, 68: 104307.

[2] Tong H, Ouyang S X, Bi Y P, Umezawa N, Oshikiri M, Ye J H. Nano-photocatalytic materials: Possibilities and challenges[J]. Adv. Mater., 2012, 24(2): 229-251.

[3] Wong E W, Sheehan P E, Lieber C M. Nanobeam mechanics: Elasticity, strength, and toughness of nanorods and nanotubes[J]. Science,1997, 277(5334): 1971-1975.

[4] Su Z J, Yang C, Xie B H, Lin Z Y, Zhang Z X, Liu J P, Li B H, Kang F Y, Wong C P. Scalable fabrication of MnO_2 nanostructure deposited on free-standing Ni nanocone arrays for ultrathin, flexible, high-performance micro-supercapacitort[J]. Energy Environ. Sci., 2014, 7(8): 2652-2659.

[5] Zhang S C, Du Z J, Lin R X, Jiang T, Liu G R, Wu X M, Weng D S. Nickel nanocone-array supported silicon anode for high-performance lithium-ion batteries[J]. Adv. Mater., 2010, 22(47): 5378-5382.

[6] Wang X H, Yang Z B, Sun X L, Li X W, Wang D S, Wang P, He D Y. NiO nanocone array electrode with high capacity and rate capability for Li-ion batteries[J]. J. Mater. Chem., 2011, 21(27): 9988-9990.

[7] Xia Y Y, Mo X, Ling H Q, Hang T, Li M. Facile fabrication of Au nanoparticles-decorated Ni nanocone arrays as effective surface-enhanced Raman scattering substrates[J]. J. Electrochem. Soc., 2016, 163(10): D575-D578.

[8] Peng Z M, Yang H. Designer platinum nanoparticles: Control of shape, composition in alloy, nanostructure and electrocatalytic property[J]. Nano Today, 2009, 4(2): 143-164.

[9] Lohse S E, Murphy C J. The quest for shape control: A history of gold nanorod synthesis[J]. Chem. Mat., 2013, 25(8): 1250-1261.

[10] Zhou X S, Wan L J, Guo Y G. Synthesis of MoS_2 nanosheet-graphene nanosheet hybrid materials for stable lithium storage[J]. Chem. Commun., 2013, 49(18): 1838-1840.

[11] Dow W P, Chen H H, Yen M Y, Chen W H, Hsu K H, Chuang P Y, Ishizuka H, Sakagawa N, Kimizuka R. Through-hole filling by copper electroplating[J]. J. Electrochem. Soc., 2008, 155(12): D750-D757.

[12] Huang Q, Lyons T W, Sides W D. Electrodeposition of cobalt for interconnect application: Effect of dimethylglyoxime[J]. J. Electrochem. Soc., 2016, 163(13): D715-D721.

[13] Moffat T P, Wheeler D, Josell D. Electrodeposition of copper in the SPS-PEG-Cl additive system-I. Kinetic measurements: Influence of SPS[J]. J. Electrochem. Soc., 2004, 151(4): C262-C271.

[14] Zheng L, He W, Zhu K, Wang C, Wang S X, Hong Y, Chen Y M, Zhou G Y, Miao H, Zhou J Q. Investigation of poly(1-vinyl imidazole co 1, 4-butanediol diglycidyl ether) as a leveler for copper electroplating of through-hole[J]. Electrochim. Acta, 2018, 283: 560-567.

[15] Dow W P, Chiu Y D, Yen M Y. Microvia filling by Cu electroplating over a Au seed layer modified by a disulfide[J]. J. Electrochem. Soc., 2009, 156(4): D155-D167.

[16] Dow W P, Lu C W, Lin J Y, Hsu F C. Highly selective Cu electrodeposition for filling through silicon holes[J]. Electrochem. Solid State Lett., 2011, 14(6): D63-D67.

[17] Gu C, Tu J. One-step fabrication of nanostructured Ni film with Lotus effect from deep eutectic solvent[J]. Langmuir, 2011, 27(16): 10132-10140.

[18] Walter E C, Zach M P, Favier F, Murray B, Inazu K, Hemminger J C, Penner R M. Electrodeposition of portable metal nanowire arrays[M]. USA: Sple-Int. Soc. Optical Engineering, 2002.

[19] Yin A J, Li J, Jian W, Bennett A J, Xu J M. Fabrication of highly ordered metallic nanowire arrays by electrodeposition[J]. Appl. Phys. Lett., 2001, 79(7): 1039-1041.

[20] Huang B H, Zhang X F, Cai J N, Liu W K, Lin S. A novel MnO_2/rGO composite prepared by electrodeposition as a non-noble metal electrocatalyst for ORR[J]. J. Appl. Electrochem., 2019, 49(8): 767-777.

[21] Wu F F, Ze H J, Chen S H, Gao X F. High-efficiency boiling heat transfer interfaces composed of electroplated copper nanocone cores and low-thermal-conductivity nickel nanocone coverings[J]. ACS Appl. Mater. Interfaces, 2020, 12(35): 39902-39909.

[22] Hang T, Hu A M, Ling H Q, Li M, Mao D L. Super-hydrophobic nickel films with micro-nano hierarchical structure prepared by electrodeposition[J]. Appl. Surf. Sci., 2010, 256(8): 2400-2404.

[23] Ebrahimi F, Bourne G R, Kelly M S, Matthews T E. Mechanical properties of nanocrystalline nickel produced by electrodeposition[J]. Nanostruct. Mater., 1999, 11(3): 343-

350.

[24] Elsherik A M, Erb U. Synthesis of bulk nanocrystalline nickel by pulsed electrodeposition[J]. J. Mater. Sci., 1995, 30(22): 5743-5749.

[25] Chen Z, Zhu C, Cai M L, Yi X Y, Li J H. Growth and morphology tuning of ordered nickel nanocones routed by one-step pulse electrodeposition[J]. Appl. Surf. Sci., 2020, 508: 145291.

[26] Lai Z Q, Wang S X, Wang C, Hong Y, Zhou G Y, Chen Y M, He W, Peng Y Q, Xiao D J. A comparison of typical additives for copper electroplating based on theoretical computation[J]. Comput. Mater. Sci., 2018, 147: 95-102.

[27] Wang C, An M Z, Yang P X, Zhang J Q. Prediction of a new leveler (N-butyl-methyl piperidinium bromide) for through-hole electroplating using molecular dynamics simulations[J]. Electrochem. Commun., 2012, 18: 104-107.

[28] Sun H, Ren P, Fried J R The compass force field: Parameterization and validation for phosphazenes[J]. Comput. Theor. Polym. Sci., 1998, 8(3-4): 363-363.

[29] Hackett J C. Chemical reactivity theory: A density functional view[J]. J. Am. Chem. Soc., 2010, 132(21): 7558-7558.

[30] Jiang Q, Tallury S S, Qiu Y P, Pasquinelli M A. Interfacial characteristics of a carbon nanotube-polyimide nanocomposite by molecular dynamics simulation[J]. Nanotechnol. Rev., 2020, 9(1): 136-145.

[31] Premkumar S, Jawahar A, Mathavan T, Dhas M K, Sathe V G, Benial A M F. Dft calculation and vibrational spectroscopic studies of 2-(tert-butoxycarbonyl (Boc) -amino) -5-bromopyridine[J]. Spectroc. Acta Pt. A-Molec. Biomolec. Spectr., 2014, 129: 74-83.

[32] Shen J, Li Y, He J H. On the Kubelka-Munk absorption coefficient[J]. Dyes Pigment., 2016, 127: 187-188.

[33] Tang M X, Zhang S T, Qiang Y J, Chen S J, Luo L, Gao J Y, Feng L, Qin Z J. 4,6-Dimethyl-2-mercaptopyrimidine as a potential leveler for microvia filling with electroplating copper[J]. RSC Adv., 2017, 7(64): 40342-40353.

[34] Oláh J, Van Alsenoy C, Sannigrahi A B. Condensed fukui functions derived from stockholder charges: Assessment of their performance as local reactivity descriptors [J]. J. Phys. Chem. A, 2002, 106(15): 3885-3890.

[35] Lai Z Q, Wang C, Huang Y Z, Chen Y M, Wang S X, Hong Y, Zhou G Y, He W, Su X H, Sun Y K, Tao Y G, Lu X Y. Temperature-dependent inhibition of PEG in acid copper plating: Theoretical analysis and experiment evidence[J]. Mater. Today Commun., 2020, 24: 100973.

[36] Saraireh S A, Altarawneh M, Tarawneh M A. Nanosystem's density functional theory study of the chlorine adsorption on the Fe(100) surface[J]. Nanotechnol. Rev., 2021, 10(1): 719-727.

[37] Tarasevich Y I. The surface energy of hydrophilic and hydrophobic adsorbents[J]. Colloid J., 2007, 69(2): 212-220.

[38] Zhu J, Yu Z F, Burkhard G F, Hsu C M, Connor S T, Xu Y Q, Wang Q, McGehee M, Fan S H, Cui Y. Optical absorption enhancement in amorphous silicon nanowire and nanocone arrays[J]. Nano Lett., 2009, 9(1): 279-282.

[39] Xu Q, Qian X, Qu Y Q, Hang T, Zhang P, Li M, Gao L. Electrodeposition of Cu_2O nanostructure on 3D Cu microcone arrays as photocathode for photoelectrochemical water reduction[J]. J. Electrochem. Soc., 2016, 163(10): H976-H981.

[40] Li M H, Keller P, Li B, Wang X G, Brunet M. Light-driven side-on nematic elastomer actuators[J]. Adv. Mater., 2003, 15(7-8): 569-572.

电沉积纳米锥镍的生长机理及其性能的研究

倪修任[1],张雅婷[1],王 翀[1],洪 延[1*],陈苑明[1],苏元章[1],何 为[1],
陈先明[2],黄本霞[2],续振林[3],李毅峰[3],李能彬[3],杜永杰[4]

(1. 电子科技大学材料与能源学院, 四川 成都 610054; 2. 珠海越亚半导体股份有限公司, 广东 珠海 519175;
3. 厦门柔性电子研究院有限公司 & 厦门弘信电子科技集团股份有限公司,福建 厦门 361101;
4. 珠海能动科技光学产业有限公司, 广东 珠海 519175)

摘要: 本文通过恒电流沉积法在柔性覆铜基板上制备了具有纳米锥阵列结构的黑色镍层, 制备的纳米锥镍的底部约为 200 nm, 高度约为 1 μm,且大小均一,分布致密。本文探讨了镍电沉积中电流密度和主盐浓度对纳米锥镍结构形貌的影响, 结果表明低电流密度和高主盐浓度有利于纳米锥镍的形成。电沉积过程中保持镍离子的供应充足是锥镍结构产生的关键因素之一, 而高电流密度会影响镍离子浓度的浓差极化,从而影响锥镍的成核过程。温度、主盐浓度以及结晶调整剂的变化会导致镍颗粒的形貌发生圆包状和针锥状结构的相互转化。温度升高具有一定的细化晶粒作用,锥镍结构需要在大于 50 ℃ 的条件下生成。结晶调整剂能够改变沉积过程中的晶面择优生长,且可以调控镍晶粒的形貌,使得生成的锥结构分布均匀, 颗粒细致。结果表明,在4.0 mol·L^{-1} NH_4Cl 和 1.68 mol·L^{-1} $NiCl_2·6H_2O$ 体系中沉积出分布均匀的纳米锥镍阵列结构。本文利用氯化铵作为纳米锥镍的晶体改性剂,通过分子动力学模拟理论上分析了 NH_4^+ 在镍表面的吸附过程。计算结果表明镍不同晶面上 NH_4^+ 吸附能的差异引起各晶面镍沉积速率的差异, 从而导致纳米锥镍阵列的形成。本文呢进一步结合形貌表征,提出了纳米锥镍阵列的电沉积生长的两步生长机理,包括前期的成核生长和后期的核生长过程,前期成核过程为优势生长,生成大量的晶核, 为锥镍的生长提供了生长位点,而后期的核生长过程表现为锥状镍核的择优生长, 最终形成完整均匀的锥镍阵列结构。本文制备的纳米锥镍结构还具有优异的亲水性和良好的吸光效果, 对于近紫外和可见光的吸收率大于 95%, 具有较好的应用前景。

关键词: 纳米锥镍阵列; 电沉积; 分子动力学模拟; 柔性